Concentration-Dependent Viscoelasticity of Poloxamer-Shelled Microbubbles

Hiraku Tabata, Daisuke Koyama, Mami Matsukawa, Marie Pierre Krafft, Kenji Yoshida

Concentration-dependent Viscoelasticity of Poloxamer-Shelled Microbubbles

Hiraku Tabata[1], Daisuke Koyama[1], Mami Matsukawa[1], Marie Pierre Krafft[2], Kenji Yoshida[3]*

[1]Faculty of Science and Engineering, Doshisha University, 1-3 Tataramiyakodani, Kyotanabe, Kyoto 610-0321, Japan

[2]Institut Charles Sadron (CNRS), University of Strasbourg, 23 rue du Loess, 67034 Strasbourg, France

[3]Center for Frontier Medical Engineering, Chiba University, 1-33 Yayoicho, Inage-ku, Chiba 263-8522, Japan

*kenyoshi1980@chiba-u.jp

Abstract:

The oscillation of shelled microbubbles during exposure to ultrasound is influenced by the mechanical properties of the shell components. The oscillation behavior of bubbles coated with various phospholipids and other amphiphiles has been studied. However, there have been few investigations of how the adsorption conditions of the shell molecules relate to the viscoelastic properties of the shell and influence the oscillation behavior of the bubbles. In the present study, we investigated the oscillation characteristics of microbubbles coated with a poloxamer surfactant, i.e., Pluronic F-68, at several concentrations after the adsorption kinetics of the surfactant at the gas–water interface had reached equilibrium. The dilatational viscoelasticity of the shell during exposure to ultrasound was analyzed in the frequency domain from the attenuation characteristics of the acoustic pulses propagated in the bubble suspension. At Pluronic F-68 concentrations lower than 2.0×10^{-2} mol L^{-1}, the attenuation characteristics typically exhibited a sharp peak. At concentrations higher than 2.0×10^{-2} mol L^{-1}, the peak flattened. The dilatational elasticity and viscosity of the shell were estimated by fitting the theoretical model to the experimental values, and revealed that both the elasticity and viscosity increased markedly at approximately 2.0×10^{-2} mol L^{-1}. This suggests that the adsorption properties of Pluronic F-68 strongly affect the oscillation characteristics of microbubbles of a size suitable for medical ultrasound diagnostics.

Introduction

Microbubbles have been used as ultrasound contrast agents, enhancing the nonlinear echoes and improving the contrast of vasculature in the acquired image. Pathophysiological ultrasound imaging has become possible thanks to the use of targeted microbubbles which can specifically adhere to the target molecule, such as P-selectin, VEGFR-2, and $\alpha_v\beta_3$[1-3]. The microbubbles, however, can target only markers within the intravascular space because they are relatively large and confined to the vasculature. Therefore, developing the targeted nanobubbles with several hundred nanometers, which can pass through intercellular space, expands the biomedical application of ultrasound[4]. In both cases

of micro- and nanobubbles, the viscoelastic properties of shell coating a gas core significantly affect the generation of the contrast echo. Sojahrood et al. numerically analyze the nonlinear behavior of microbubbles with a model that can describe membrane buckling and rapture[5]. The other work by Sojahrood et al experimentally found a specific sound pressure dependence of nonlinear echoes from nanobubbles and showed that the threshold depends on the shell structure[6]. Leon showed superior contrast effects of nanobubbles in an in-vivo study, where half-life was prolonged compared with microbubbles[4].

On the other hand, micro- and nanobubbles are also potentially useful for other therapeutic applications[7–13], such as the targeted delivery of drugs in the brain[14]. In medication, the control of vascular permeability determines therapeutic efficacy. The brain has a specialized vascular endothelial system called the blood–brain barrier (BBB). The capillary endothelial cells of the brain have tight junctions that protect it from harmful agents and control the transportation of substances[15]. However, the efficacy of brain tumor drugs is limited owing to their inability to permeate the blood vessels. To solve this issue, a method combining ultrasound and microbubbles was demonstrated to improve the permeation of drugs through the BBB[16–18]. One possible explanation for why this strategy is effective is that the oscillation of the bubbles causes reversible perforation[19]. When a bubble adhering to the endothelial cells contracts, the cell membrane is pulled by that bubble and subjected to shear stress by the surrounding fluid. During expansion, the bubble pushes on the cell membrane. The destruction of the bubbles also make the path through the drug[20]. These stresses result in the perforation of the cell membrane, which increases drug permeability[15,21]. Therefore, the destruction behavior and the oscillation characteristics of the bubble are important determinants of drug permeability and require further study.

In therapeutic applications and diagnostic imaging, bubbles need to circulate through the body for an extended period of time. Therefore, it is important that they are highly stable. Perfluorocarbons are inert with regard to biological systems[13,22], and are frequently used as the core gases of the microbubbles. They are extremely insoluble in water, which stabilizes the bubble[22-24]. The soft shell that coats the bubble also plays a role in stabilization. A theoretical model for the diffusion of gas bubbles in liquids was developed by Epstein and Plesset[25]. The resistance term of the diffusion by the shell is then considered and the diffusion behavior of bubbles coated with a lipid is studied[26]. To further suppress gas diffusion, a two-layered shell was investigated, which showed high stability in nanobubbles[15]. As stated above, however, the shell composition greatly affects its viscoelasticity, i.e., causes a shift of the resonance frequency, damping of the oscillation amplitude and changing the destruction propensity. These effects have been investigated theoretically and experimentally[27–30]. The acoustic characteristics of the commercial microbubbles Sonazoid™ (Daiichi Sankyo, GE Healthcare, Tokyo, Japan), Definity® (Lantheus, North Billerica, MA, USA), and SonoVue® (Bracco, Milan, Italy) have been investigated by measuring the attenuation of acoustic pulse waves, and the

dilatational viscoelasticity values of these shells have been estimated using a theoretical model[31–33]. More precisely, phospholipids with carbon chains of various lengths were used as the shell and their effects were examined[34,35]. Poloxamer surfactants are often used to prepare laboratory-made and commercial phospholipid-based microbubbles[28,34]. The acoustic properties of bubbles coated with shells containing various ratios of lipids and poloxamer surfactants have been reported in several studies[28,34,36,37]. However, there are few reports on the acoustic properties of bubbles coated with poloxamer surfactants used as the only shell material. In addition, the relationships between the adsorption properties of the shell material and its dilatational viscoelasticity have not been investigated.

In a previous study, we investigated the adsorption kinetics of various concentrations of Pluronic-F68 at the perfluorocarbon-saturated interface with water. At least two phase transitions caused by different anchoring of the molecules at the interface were evident depending on the Pluronic F-68 concentration[38]. We also evaluated the resonance radius and the maximum oscillation amplitude of single Pluronic F-68-shelled bubbles with radii varying from 20 to 150 μm using an optical observation system during exposure to ultrasound[24]. The oscillation behavior was hardly affected by the coating with Pluronic F-68 molecules, although the theory of bubble dynamics generally predicts that the resonance radius is increased by shell dilatational elasticity, and the oscillation amplitude is dampened by the dilatational viscosity. We hypothesized that the effect of the dilatational elasticity may be canceled by the decrease in surface tension caused by Pluronic F-68, and that the effect of dilatational viscosity is masked by the dominating damping factor of thermal damping[39].

The present report focuses on bubbles with radii of a few micrometers that are applicable to ultrasound-based medical applications. During exposure to ultrasound, any difference in the adsorption properties of the shell-forming molecules may result in an observable change in the oscillation characteristics. The oscillation characteristics of the Pluronic F-68 microbubbles were determined from the attenuation characteristics of the acoustic pulses propagating in the bubble suspensions. First, we analyzed the change in the attenuation characteristics for each concentration as for estimating the effect of the Pluronic F-68 shell. We then quantified the dilatational viscoelasticity of the Pluronic F-68 shell by fitting the theoretical prediction to the experimentally measured attenuation. Herein, we discuss how the viscoelasticity of the Pluronic F-68 shell depends on its concentration, i.e., on its adsorption properties.

Experimental Section

Preparation of poloxamer solution

Pluronic F-68 was purchased from Sigma-Aldrich [$(PEO)_A(PPO)_B(PEO)_A$; CAS Registry No. 9003-11-6; molecular weight (M_w) of ~8400 g mol^{-1} according to the supplier and ~9050 g mol^{-1} according to our light scattering experiments]. The degree of polymerization of each block ($N_A = 2 \times 76$, and $N_B = 29$) was calculated from the nominal value of the M_w. The polydispersity index ($M_w/M_n = 1.15$,

where M_n is the number-average molecular weight) was obtained by gel permeation chromatography using tetrahydrofuran as a solvent. Pluronic F-68 was the sole surfactant for the microbubble coating. Ultrapure water was obtained from Arium Mini plus (H20-MA-UV-T, Sartorius, Germany). The oxygen saturation was measured using a dissolved oxygen meter (FDO380, AS ONE, Osaka, Japan), and was 95-98%.

Preparation of the microbubbles

Microbubbles coated with Pluronic F-68 were fabricated using two syringes. One syringe was filled with 5 mL of aqueous Pluronic F-68 prepared at various concentrations (from 5.0×10^{-5} to 5.0×10^{-2} mol L^{-1}). The other syringe was filled with 5 mL of air saturated with perfluorohexane (PFH). The PFH was purchased from Sigma-Aldrich and was used as a component of the microbubble gas core. The two syringes were joined via a connector and alternately pressed 50 times to prepare each bubble suspension. Each suspension was sonicated for 1 min using an NR-50M ultrasound homogenizer (MICROTEC, Japan) to control the size distribution, and was divided into three layers according to buoyancy over time. The three layers consisted of a solution layer on the bottom, a bubble layer in the middle, and a foam layer at the top. A previous study by our group revealed that the adsorption kinetics of Pluronic F-68 at the gas–water interface reached equilibrium in 10 min[38]. Therefore, we allowed the bubble suspensions to stand for 10 min after sonication. We then collected bubbles from the solution layer to obtain small and narrow size distributions.

Evaluation of the microbubble size distribution

The bubble suspensions were investigated using a bright-field microscope (VH-Z100UT, Keyence, Osaka, Japan) with an objective lens (600× magnification) (VHX-7000, Keyence, Osaka, Japan). The size distributions were analyzed from the optical images by MATLAB (The MathWorks, Natick, MA, USA). A hemocytometer, i.e. bubble chamber, was filled with 20 μl of bubble suspension. We left the chamber to stand for several minutes until the bubbles were buoyant. The focus of the optical microscopy was located on the lower surface of the glass covered with the chamber. The length per pixel in the optical images is 0.27 μm, which is much smaller than the bubbles. Several images were taken in a single trial to capture a wide area with sufficient resolution. The time taken to capture the image was within a few tens of seconds, so the change in bubble size was minimized. Figure 1 shows the typical size distribution of microbubbles coated with Pluronic F-68 of several concentrations. The solid lines show the curves fitted by the generalized extreme value distribution. The probability density function f for the generalized extreme value distribution is expressed by the following equation[40]:

$$f = \left(\frac{1}{\theta}\right) exp\left(-\left(1+\xi\frac{(r-M)}{\theta}\right)^{-\frac{1}{\xi}}\right)\left(1+\xi\frac{(r-M)}{\theta}\right)^{-1-\frac{1}{\xi}}, \quad (1)$$

where θ, ξ, and M are the location parameter, the scale parameter, and the shape parameter of the fitting parameters, respectively; r is the radius of a bubble. Table 1 summarizes the number of trials (n), the number of the bubbles, the surface tension at equilibrium, and the fitting parameters for the

normalized size distribution of bubbles at each concentration. The attenuation characteristics were obtained from the same sample used for the size distribution measurements.

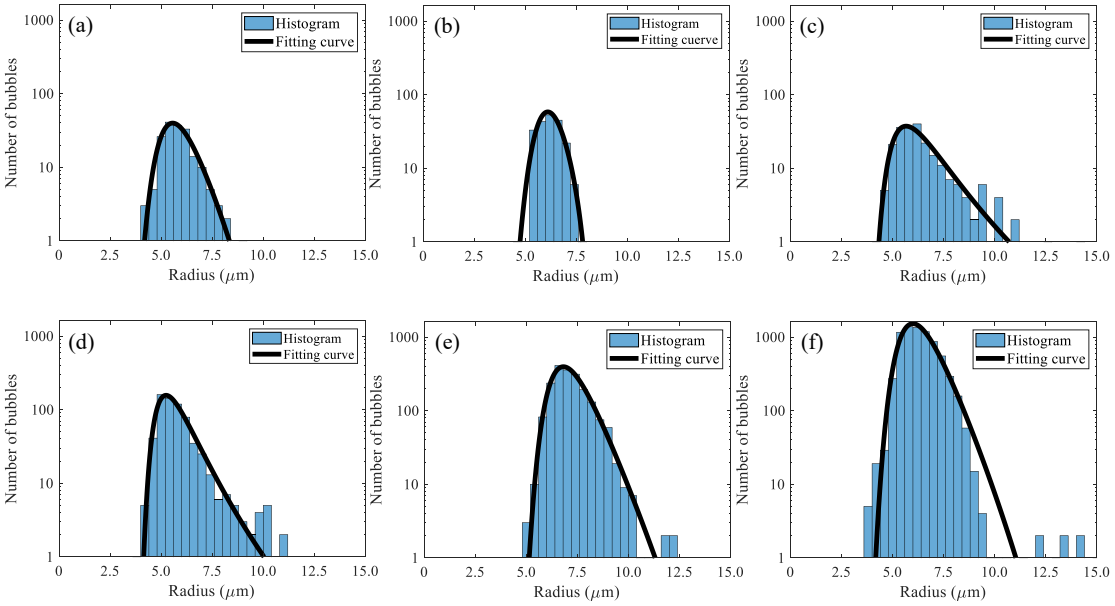

Figure 1. Typical distributions of the radii of microbubbles coated with Pluronic F-68 of concentrations (a) 5.0×10^{-5} mol L^{-1}, (b) 1.0×10^{-4} mol L^{-1}, (c) 1.0×10^{-3} mol L^{-1}, (d) 1.0×10^{-2} mol L^{-1}, (e) 2.0×10^{-2} mol L^{-1}, and (f) 5.0×10^{-2} mol L^{-1}. The solid lines are fitting curves obtained from the generalized extreme value distributions.

Table 1. The surface tension at equilibrium measured by axisymmetric drop shape analysis (ADSA) and reported previously[38], the number of trials (n), the number of bubbles, the average maximum radius in size distribution, and the fitting parameters for the generalized extreme value distribution for the bubble size distribution at each concentration.

				Bubble size distribution			
				Average radius of maximum in size distribution [μm]	Fitting parameters		
Concentration [mol L^{-1}]	Surfacetension [mN m^{-1}]*	n	Number of bubble		Location parameter (θ)	Scale parameter (ξ)	Shape parameter (M)
5.0×10^{-5}	46.0 ± 0.5	7	187 ± 76	6.84 ± 0.80	6.53 ± 0.81	0.99 ± 0.30	-0.13 ± 0.08
1.0×10^{-4}	45.0 ± 0.6	8	173 ± 57	6.17 ± 0.57	5.98 ± 0.58	0.86 ± 0.25	-0.20 ± 0.11
1.0×10^{-3}	40.0 ± 0.5	8	155 ± 47	5.49 ± 0.91	5.56 ± 0.87	0.81 ± 0.23	0.11 ± 0.13
1.0×10^{-2}	35.0 ± 0.5	7	2506 ± 3608	4.88 ± 0.32	4.80 ± 0.42	0.59 ± 0.20	0.13 ± 0.08
2.0×10^{-2}	33.0 ± 0.4	17	1540 ± 1155	6.97 ± 0.66	6.99 ± 0.65	0.79 ± 0.17	0.02 ± 0.11
5.0×10^{-2}	32.0 ± 0.5	8	5449 ± 3141	5.85 ± 0.49	5.84 ± 0.45	0.94 ± 0.18	-0.01 ± 0.05

*Surface tensions are referred to in reference 29.

Linearized model of the oscillation of a bubble coated with surfactant

Several models describe the radial oscillation of a bubble exposed to ultrasound. A modified Rayleigh-Plesset-type equation that includes elasticity and friction shell parameters was developed by de Jong et al.[41]. This theory was enhanced by Church[42] and by Hoff et al.[41] by considering the shell thickness and surface tension. Chatterjee and Sarkar assumed that the shell was of infinitesimal thickness, and that the structure of the shell in the thickness direction was nonhomogeneous and anisotropic[43]. Nonlinear oscillations such as compression-only behavior with increasing sound pressure were modeled by Marmottant et al.[44]. We used a linearized version of the Chatterjee and Sarkar model[43] to estimate the dilatational elasticity E^S and viscosity κ^s of the Pluronic F-68 shell during small amplitude oscillations.

For a bubble of radius r experiencing oscillations, it is hypothesized that the oscillation amplitude Δr will be much smaller than the initial bubble radius r_0 [$r = r_0 + \Delta r = r_0 (1 + \varepsilon)$, $\varepsilon << 1$]. The theoretical model is defined as follows:

$$\ddot{\varepsilon} + \frac{1}{\rho r_0^2}\left(4\mu + \frac{4\kappa^S}{r_0}\right)\dot{\varepsilon} + \frac{1}{\rho r_0^2}\left(3kP_0 - \frac{4\sigma_0}{r_0} + \frac{4E^S}{r_0}\right)\varepsilon = \frac{P_A}{\rho r_0^2}\sin\omega t, \quad (2)$$

where ρ is the density of the surrounding fluid, k is the specific heat ratio of the internal gas, μ is the viscosity coefficient, P_0 and P_A are the ambient pressure and pressure amplitude of sound, respectively, σ_0 is the surface tension obtained from a previous experiment[38], κ^s and E^s are the dilatational viscosity and elasticity of the shell, respectively, ω is the angular frequency, and t is time.

An acoustic pulse loses energy as it propagates through the bubble suspension. This energy loss results from the sound re-radiation by the microbubbles ($\delta_{radiation}$), the damping of the surrounding liquid (δ_{liquid}), a shell viscosity contribution ($\delta_{interface}$), and thermal damping (δ_{therm}). It can be calculated from the extinction cross section (ECS), which indicates the attenuation per bubble. The fitting curves of the generalized extreme value distribution, shown in Figure 1, were used to account for the distribution of bubbles actually fed into the experimental cell. Based on the ECS and scatter cross section (SCS) obtained from the sound field and scattering intensity, the resonance angular frequency ω_0 and damping coefficients are defined as follows:

$$\omega_0^2 = \frac{1}{\rho r_0^2}\left(3kP_0 - \frac{4\sigma_0}{r_0} + \frac{4E^S}{r_0}\right), \quad (3)$$

$$\delta_{\text{liquid}} = \frac{4\mu}{\rho\omega_0 r_0^2},\ \delta_{\text{interface}} = \frac{4\kappa^S}{\rho\omega_0 r_0^3},\ \delta_{\text{radiation}} = \frac{\omega^2 r_0}{\omega_0 c}, \quad (4)$$

where c is the speed of sound in the surrounding liquid. According to previous research, the thermal damping is approximately equal to the viscous damping during the conditions associated with medical diagnosis[28,45]. Therefore, the total damping coefficient is expressed as $\delta_{tot} = 2\delta_{liquid} + \delta_{interface} + \delta_{radiation}$. The least squares method was used to fit the theoretical model to the measured attenuation

characteristic. The dilatational elasticity and viscosity were determined so that the error Err(N, κ^S, E^S) between the theoretically calculated attenuation and the experimental value in the 0-2 MHz frequency range was minimized. The error is defined by the following equation:

$$Err(\mathrm{N}, \kappa^s, E^s) = \sum_i [\alpha_{\mathrm{theo}}(\omega_i) - \alpha_{\mathrm{bubble}}(\omega_i)]^2, \quad (5)$$

where $\alpha(\omega_i)_{\mathrm{theo}}$ and $\alpha(\omega_i)_{\mathrm{bubble}}$ are the attenuation characteristics obtained from the theoretical model and the experiments, respectively, N is the sum, and ι is an arbitrary constant.

Measurement of attenuation coefficient

Measuring the attenuation and scattering of ultrasound waves is a simple way of estimating the dilatational viscoelasticity of the shell. Figure 2 shows the system used for measuring the attenuation characteristics of ultrasound. A cubic cell (30 × 30 × 30 mm) was filled with an aqueous solution of Pluronic F-68, and an acrylic block was placed on the bottom as a reflector. The concentration of Pluronic F-68 was the same as that used to prepare the bubbles. This was done to maintain the adsorbed Pluronic F-68 molecules in equilibrium[46,47]. A plane transducer (V303, Olympus, Tokyo, Japan) for transmitting and receiving waves was placed 10 mm from the reflector, and excited using a pulser/receiver (Model 5800, Olympus, Tokyo, Japan) via an attenuator (FAT-5030B, Nidec Copal Electronics Corp., Tokyo, Japan). The frequency of the pulsed ultrasound wave at peak amplitude was 1 MHz. The negative peak sound pressure at the center of the observation cell, which was measured using a 0.2 mm needle hydrophone (Precision Acoustic, Dorchester, UK) with an effective frequency range of 0–30 MHz, was approximately 4 kPa. Such pressure conditions ensure that the linear oscillation of the bubble is suitable for fitting to estimate the viscoelasticity of the shell[28,36]. While there are some concerns with the estimation of the dilatational viscoelasticity and oscillation behavior by the broadband attenuation measurement of ultrasound, the estimated value are highly reliable at low sound pressure, such as our experimental conditions[48,49]. A highly precise tri-axis stage connected to a bi-axis goniometer was used to control the position and angle of the transducer.

First, the Pluronic F-68 aqueous solutions without bubbles were submitted to acoustic pulses. Pulsed sound waves (1 MHz) were repeatedly emitted 10,000 times for 2 s with a pulse repetition frequency of 5 kHz, and the corresponding reflected signals were recorded as reference signals using a oscilloscope (5444D MSO, Pico Technology, Wales, England) wherein the vertical resolution was an 8 bit quantization. The sampling frequency of the oscilloscope was 1 GHz and after down sampling, the sampling frequency was 9.6 MHz when storing the data. The collective average of received waves improved the signal-noise ratio. The power spectra were obtained from the Fourier transform of the averaged signal. Subsequently, a few tens of microliters of bubble suspension were injected into the experimental cell. The samples of injected bubble suspensions were the same as those used for measuring the bubble size distributions. The lifetimes of the bubbles increase as the concentration increases[38]. Therefore, the number density of the bubble suspension changed with concentration. The

amount of bubble suspension was adjusted so that it was appropriate for measuring attenuation at each Pluronic F-68 concentration. The reflected signal in the presence of bubbles was obtained and analyzed according to the same procedure used to measure the reference signal. Each experiment was conducted at 22.0 ± 1.0 °C. Figure 3 shows the typical waveforms and frequency spectra in the presence and absence of bubbles. The attenuation coefficient α was calculated using the following equation:

$$\alpha(f) = -8.686\frac{1}{4d}\log_{10}\frac{P(f)}{P_{\mathrm{ref}}(f)}, \tag{6}$$

where P and P_{ref} are the average power spectra in the presence and absence of bubbles, respectively, and d is the distance between the transducer and the reflector.

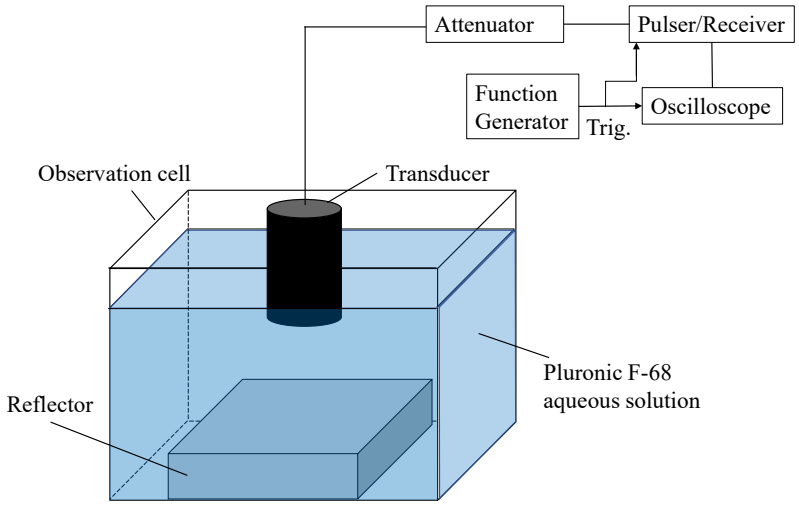

Figure 2. System used for measuring the acoustic pulse using a pulser/receiver and a transducer.

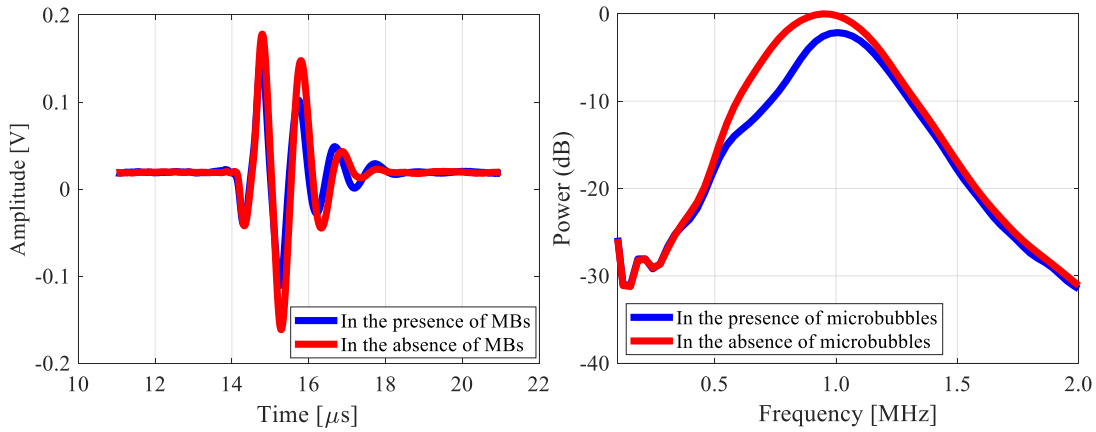

Figure 3. Typical signals and frequency spectra of the reflected waves in the presence and absence of bubbles.

Results and Discussion

Attenuation characteristics

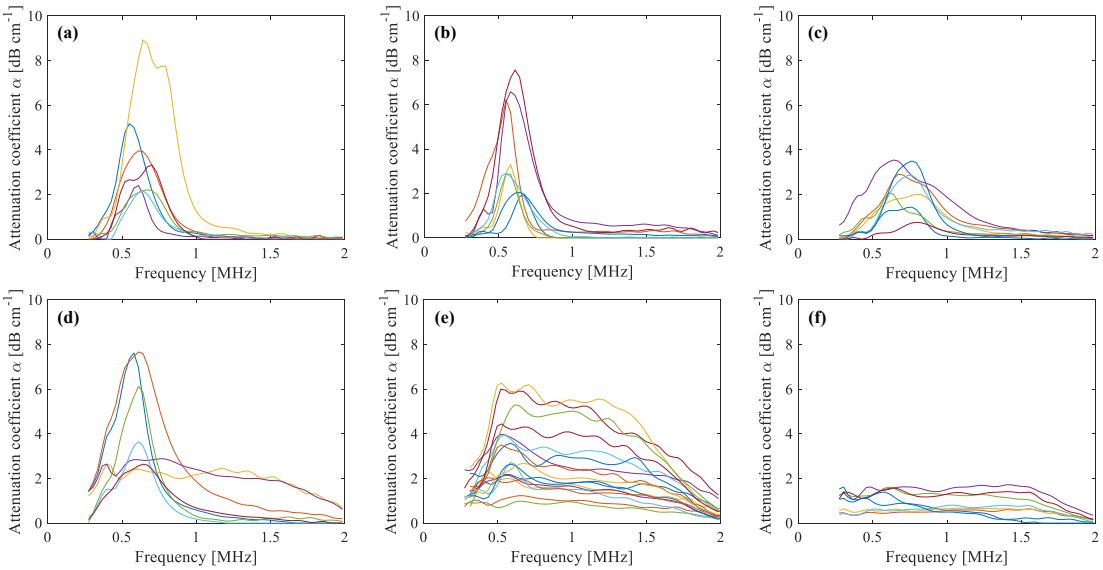

Figure 4. Frequency characteristics of attenuation at several Pluronic F-68 concentrations. The trials were conducted: (a) 7 times at 5.0×10^{-5} mol L^{-1}, (b) 8 times at 1.0×10^{-4} mol L^{-1}, (c) 8 times at 1.0×10^{-3} mol L^{-1}, (d) 7 times at 1.0×10^{-2} mol L^{-1}, (e) 17 times at 2.0×10^{-2} mol L^{-1}, and (f) 8 times at 5.0×10^{-2} mol L^{-1}. The solid lines are color-coded for each trial.

The oscillations of the bubbles were evaluated by characterizing the attenuation coefficient. Figure 4 shows the analyzed attenuation characteristics at several Pluronic F-68 concentrations. The vertical axis represents the attenuation coefficient α, as defined in Eq.6. The solid colored lines represent the average attenuation characteristics of an acoustic pulse repeatedly emitted 10,000 times in one trial, and are color-coded for each trial.

For low concentrations (5.0×10^{-5} to 1.0×10^{-3} mol L^{-1}), there was a sharp peak in the attenuation characteristic at 600-700 kHz. However, the peak flattened out over a wide frequency band at higher concentrations (2.0×10^{-2} mol L^{-1} and 5.0×10^{-2} mol L^{-1}). This was not clearly caused by the difference in the sizes of the bubbles, because there were few differences in the microbubble size distributions. As shown in Figure 1, comparing 5.0×10^{-5} mol L^{-1} with 2.0×10^{-2} mol L^{-1}, and 1.0×10^{-3} mol L^{-1} with 5.0×10^{-2} mol L^{-1}, the differences in the mean diameters of the bubbles are approximately 0.13 and 0.36 μm, respectively. A quadratic function was used to evaluate the differences in the attenuation characteristics, and it was fitted over the frequency band where the attenuation coefficient was half the value of the peak value. When the attenuation characteristic was flat, the quadratic function was fitted over the widest frequency band because there was no sharp peak. The coefficient of determination (R^2) for the fitting of the quadratic function was calculated at each

concentration, and the number of data with $R^2 < 0.95$ were scored. Table 2 summarizes the average coefficients obtained for the fitting, the numbers of data below threshold, and their ratios. The average coefficients of the determination decreased as the concentration increased, and all the data for concentrations of 2.0×10^{-2} mol L^{-1} and 5.0×10^{-2} mol L^{-1} were below the threshold. These data strongly pointed that the attenuation characteristics changed with PluronicF-68 concentrations. Figure 5 (a) and (b) shows representative examples of the fitting curves and attenuation characteristics measured at low (5×10^{-5} mol L^{-1}) and high (5×10^{-2} mol L^{-1}) concentrations, where the coefficient of determination for the fitting curve is highest at the respective concentrations. A previous study showed that bubble-bubble interaction was an important factor affecting the attenuation characteristics, which was determined by void fraction β [50,51]. The void fraction was estimated assuming that the bubble size distribution was uniform in our experimental cell, and summarized in the table 3. Previous studies have simulated that low values of void fraction($\beta < 10^{-7}$) have little effect on attenuation characteristics[52]. At high Pluronic F-68 concentration, the void fraction was relatively high, indicating that the attenuation characteristics may have been weakly affected by bubble-bubble interactions. The void fractions in our experimental conditions are smaller than 10^{-5} at least. Even if there was an effect, the change in attenuation characteristics owing to bubble-bubble interaction was different from our data. In the previous study, theoretical calculation pointed out that bubble-bubble interaction slightly shifted the attenuation characteristic to a lower frequency at $\beta = 10^{-6}$ and $r_0 = 2$ μm. In contrast, the notable trend observed in Figs. 4 and 5 was the broadening of attenuation characteristic. Therefore, it was suggested that the change of attenuation characteristic in our data resulted from the concentration of Pluronic F-68, not bubble-bubble interaction.

It should be noted that at the boundary concentration (1.0×10^{-2} mol L^{-1}), where the attenuation characteristic changed from that shown in Figures 5 (a) to that shown in Figure 5 (b), both types of attenuation characteristics were confirmed. Because the critical micelle concentration (CMC) was around 1.0×10^{-2} mol L^{-1}[53,54,55], the micelle condition may have been affected. Adsorption kinetics are affected by concentration, temperature, and the presence or absence of micelles[46]. In trials conducted at the CMC, sonication during the bubble production process disrupted the micelles; this may have changed the adsorption kinetics resulting in different attenuation characteristics[46].

Yoshida et al. have reported such a change in the attenuation characteristics in the case of phospholipid-coated bubbles as shown in Figure 5 (a) and 5 (b)[45]. They prepared two types of bubbles. One type was coated with 2-distearoyl-*sn*-glycero-3-phosphocholine (DSPC), resulting in attenuation characteristics similar to those depicted in Figure 5 (b). The other type was coated with a mixture of DSPC and various types of phospholipids including lecithin and cholesterol, resulting in characteristics similar to those shown in Figure 5 (a). The authors speculated that a gel-phase shell was formed in the former case and that a liquid-crystalline or fluid-phase shell was formed in the latter case. Our results suggest that a phase transition occurred in the shell that depended on the

concentration of Pluronic F-68.

Table 2. The average coefficient of determination for fitting, the number of excluded data, and their ratios.

Concentration [mol L^{-1}]	n	Coefficient of determination (R^2) [Average ± standard deviation]	Number of data below threshold	Ratio of data below threshold [%]
5.0×10^{-5}	7	0.91 ± 0.10	3	42
1.0×10^{-4}	8	0.94 ± 0.08	3	37
1.0×10^{-3}	8	0.89 ± 0.12	5	62
1.0×10^{-2}	7	0.83 ± 0.20	4	57
2.0×10^{-2}	17	0.63 ± 0.16	17	100
5.0×10^{-2}	8	0.60 ± 0.20	8	100

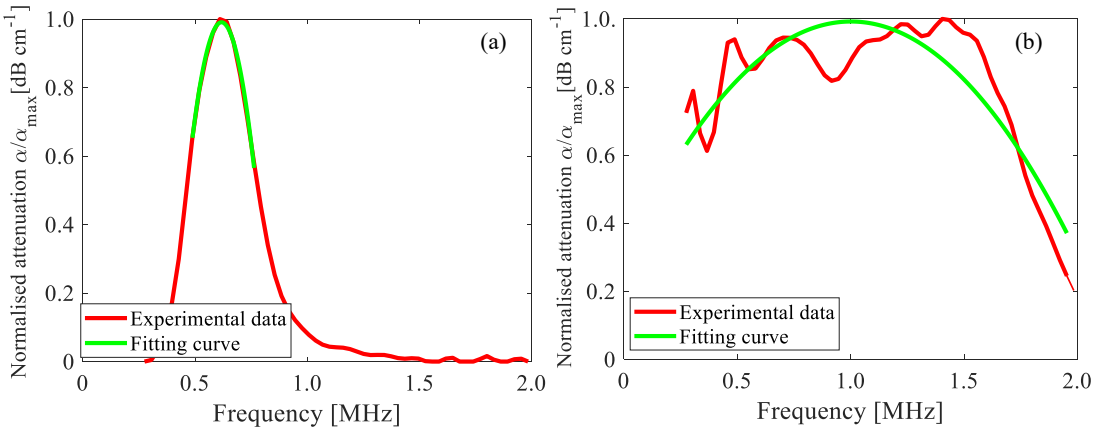

Figure 5. Typical attenuation characteristics measured at low and high Pluronic F-68 concentrations. The solid red lines represent the experimental values, and the solid green lines represent the fitting curves obtained from the quadratic function. (a) and (b) represent Pluronic F-68 concentrations of 5×10^{-5} mol L^{-1} and 5×10^{-2} mol L^{-1}, respectively.

Table 3. The void fraction and the number density of bubbles for each concentration at the attenuation measurement.

Concentration [mol L^{-1}]	Number density of bubble [MBs m^{-3}]	Void fraction β [%]
5.0×10^{-5}	$(3.0 \pm 1.2) \times 10^{8}$	$(4.4 \pm 1.3) \times 10^{-7}$
1.0×10^{-4}	$(2.8 \pm 0.92) \times 10^{8}$	$(2.9 \pm 1.2) \times 10^{-7}$
1.0×10^{-3}	$(2.5 \pm 0.77) \times 10^{8}$	$(2.9 \pm 1.4) \times 10^{-7}$
1.0×10^{-2}	$(4.1 \pm 5.9) \times 10^{9}$	$(1.4 \pm 1.6) \times 10^{-6}$

2.0×10^{-2}	$(2.5 \pm 1.9) \times 10^{9}$	$(4.3 \pm 2.8) \times 10^{-6}$
5.0×10^{-2}	$(8.9 \pm 5.1) \times 10^{9}$	$(1.1 \pm 0.68) \times 10^{-5}$

Viscoelastic properties of the shell formed on the bubble surface

The dilatational elasticity and viscosity values of the shells formed at various Pluronic F-68 concentrations were obtained by fitting the Sarkar model to the attenuation characteristics. The oscillation of bubbles coated with lipid shells changes from linear to nonlinear as the sound pressure increases. In the nonlinear regime, the lipid shell buckles during contraction and ruptures during expansion[56,57], indicating that the dilatational viscoelasticity of the shell during nonlinear oscillation dynamically changes synchronizing with its oscillation, and thus the estimated value should be misestimated to be different from that during linear oscillation[14,56,58]. Several research demonstrated that bubbles coated with a lipid shell oscillate linearly at a sound pressure of 20 kPa, and exhibit moderate nonlinear oscillation at 50 kPa[25,52]. Other research group show that lipid-coated bubbles exhibited nonlinear oscillations as sound pressure increased from 12.5 to 25 kPa[50]. Although their threshold was greatly affected by the shell material and fabrication method, it is reasonable to assume that the oscillation of the Pluronic F-68 bubbles in our experiment was linear. This is because the sound pressure was low in our system (4 kPa). Figure 6 shows dilatational elasticity and viscosity as functions of the bubble radius, as determined from the maximum of the size distribution evaluated from the optical microscopy results. For each trial at 5.0×10^{-5} mol L^{-1} and 1.0×10^{-4} mol L^{-1}, the viscosity was so small that it could not be determined from the data from the four trials. The size dependency of the viscoelasticity of lipid-coated microbubble shells has been reported previously[27,28,29,36]. It has been hypothesized that this phenomenon is caused by shear-thinning and strain-softening. The research has also shown that the dilatational viscoelasticity of the shells of lipid-coated bubbles tends to be negatively correlated with the shear rate and deformation strength when the sound pressure is high enough to cause nonlinear oscillation (as in the case of compression-only behavior)[36]. However, other reports suggest that there are no such significant correlations, regardless of whether the oscillation behavior is linear or nonlinear[28,34]. In order to examine whether our experimental results also show the size dependency, Spearman's correlation coefficients were calculated. As a result, no significant correlation could be shown for both the dilatational viscosity and the dilatational elasticity. This may be due to the polydispersity of the bubble size distribution that reduced the accuracy of the measurement[13]. Higher precision measurement may be required to verify the size dependence of Pluronic F-68 bubbles.

Figure 7 shows the variations in the average dilatational elasticity and viscosity of bubbles with radii ranging from 5 to 6 μm versus Pluronic F-68 concentration. In Figure 7 (a) and (b), the plots for 5×10^{-5} mol L^{-1}, 1.0×10^{-4} mol L^{-1} (the dilatational viscosity only), 1.0×10^{-2} mol L^{-1}, and 2.0×10^{-2} mol L^{-1} have no error bars because the number of valid trials in which the maximum size distribution

ranged from 5 to 6 μm was 1 or 2. The data obtained at a Pluronic F-68 concentration of 1.0×10^{-1} mol L^{-1} revealed attenuation characteristics with sharp peaks similar to that shown in Figure 5 (a). It should be noted that the average dilatational elasticity and viscosity at 2.0×10^{-2} mol L^{-1} increased by approximately 3- and 40-fold, respectively, relatively to concentrations below 1.0×10^{-2} mol L^{-1}. As reported in a study of the adsorption kinetics of Pluronic F-68 at a gas-water interface (the gas being air or perfluorohexane-saturated air)[38], in the concentration range used in the present experiment, the hydrophilic segments of the Pluronic F-68 molecules oriented toward the liquid phase. Maintaining that orientation, the density of the molecules at the gas-water interface increased as the Pluronic F-68 concentration increased, which left no space for the additional adsorption of molecules at equilibrium at a concentration of 1.0×10^{-2} mol L^{-1}[38,47]. The dilatational elasticity increased as the adsorbed molecules formed a dense shell. The densely packed molecules rubbed against each other during radial oscillation, resulting in an increase in the dilatational viscosity. Therefore, the shell transitioned from a fluid phase to a solid phase (the gel phase), depending on the density of the adsorbed molecules.

In the present study, the estimated dilatational elasticity and viscosity values were much larger than those previously reported for lipid-coated microbubbles ($E^s \leq 1$ N m^{-1} and $\kappa^s \leq 10^{-7}$ N s m^{-1}, respectively)[27,28,32,34]. The significantly larger viscoelasticity may be attributed to the density of the adsorbed molecules and their effective lengths in the thickness direction of the shell.

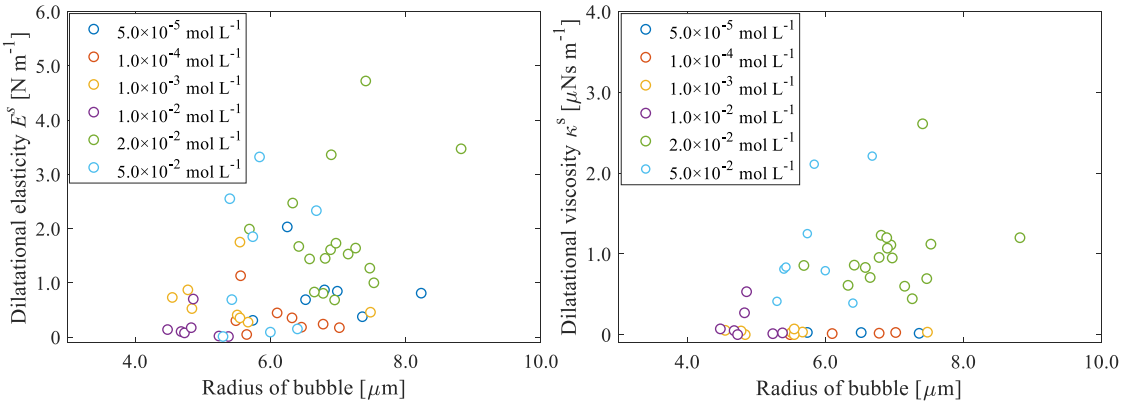

Figure 6. Variation in (a) dilatational elasticity *Es* and (b) viscosity κ^s as functions of the microbubble radius. *Es* and κ^s were estimated from the attenuation characteristics by fitting a theoretical model.

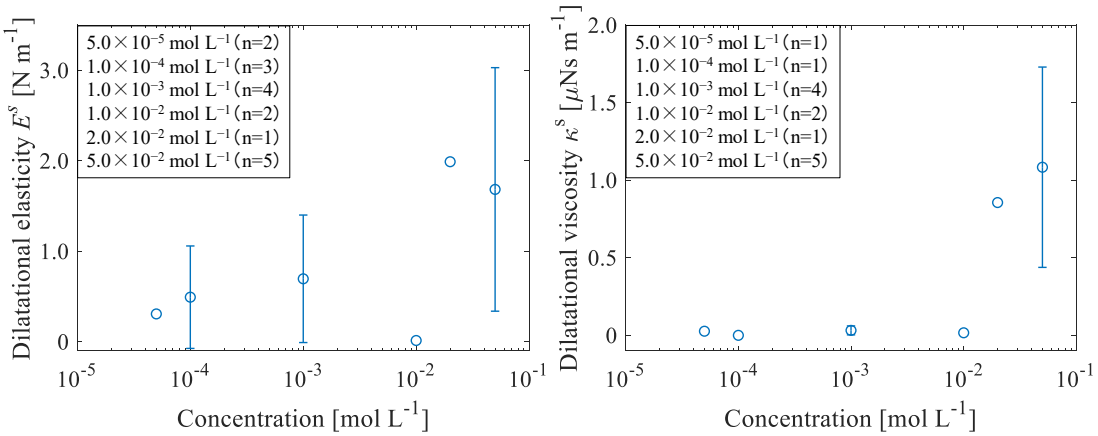

Figure 7. Variation in the average dilatational elasticity *Es* and viscosity κ^s of the bubbles as functions of Pluronic F-68 concentration for microbubbles with radii ranging from 5 to 6 μm, as shown in Figures 6 (a) and (b).

Conclusions

Microbubbles prepared at several Pluronic F-68 concentrations were investigated to determine the oscillation characteristics and dilatational viscoelasticity values of the bubble shells when exposed to low sound pressure ultrasound. In a previous study on large bubbles (a few tens of micrometers), the concentration of Pluronic F-68 forming the shell had no effect on the oscillation characteristics. However, at bubble sizes with potential clinical applicability, the oscillation characteristics and dilatational viscoelasticity values of the bubble shells, which were estimated from the attenuation characteristics of acoustic pulses, were strongly related to the Pluronic F-68 concentration. Our study showed that the dilatational elasticity and viscosity increased substantially when the adsorbed molecules reached saturation at the perfluorohexane-saturated air/water interface. This implies that a phase transition occurred in the shells. At the concentration ranges used in the present study, the hydrophilic segments of the adsorbed Pluronic F-68 molecules oriented toward the liquid phase, whereas the molecules were flat at the interface in the low concentration region. The effect of the difference in orientation of the hydrophilic and hydrophobic segments requires further investigation because the interaction of the adsorbed molecules with respect to the radial direction changes.

Acknowledgments

We thank Frank Kitching, MSc., from Edanz (https://jp.edanz.com/ac) for editing a draft of this manuscript. We thank Goho Life Science (Japan) for travel grants. This work was partly supported by JSPS KAKENHI (grant number JP19H04436).

References

(1) Klibanov, A. L. Ultrasound Molecular Imaging of Cancer: Design and Formulation Strategies of Targeted Contrast Agents. *Mol Imag Oncol.* **2020**, *216*, 319–336.

(2) van Rooij, T.; Daeichin, V.; Skachkov, I.; de jong, N.; Kooiman, K. Targeted ultrasound contrast agents for ultrasound molecular imaging and therapy. *Int J Hyperthermia* **2015**, *31(2)*, 90-106..

(3) Langeveld, S. A. G.; Meijlink, B.; Kooiman, K. Phospholipid-coated targeted microbubbles for ultrasound molecular imaging and therapy. *Curr. Opin. Chem. Eng.* **2021**, *63*, 171–179.

(4) de Leon, A.; Perera, R.: Cooley, M.; Jung,O.; Jeganathan, S.; Abenojar, E.; Fishbein, G.; Sojahrood, A. J.; Emerson, C.C.; Kolios, M. C.; Exner, A. A. Contrast enhanced ultrasound imaging by natureinspired ultrastable echogenic nanobubbles *Nanoscale* **2019**, *11(33)*, 15647-15658.

(5) Sojahrood, A. J.; Haghi, H.; Karshafian, R.; Kolios, M. C. Nonlinear dynamics and bifurcation structure of ultrasonically excited lipid coated microbubbles. *Ultrason Sonochem*, **2021**, *72*.

(6) Sojahrood, A. J.; de Leon, A. C.; Lee, R.; Cooley, M.; Abenojar, E. C.; Kolios, M. C.; Exner, A. A. Toward precisely controllable acoustic response of shell-stabilized nanobubbles: High yield and narrow dispersity. *ACS nano* **2021**, *15*(3), 4901-4915.

(7) Suzuki, R.; Takizawa, T.; Negishi, Y.; Utoguchi, N.; Sawamura, K.; Tanaka, K.; Namai, E.; Oda, Y.; Matsumura, Y.; Maruyama, K. Tumor specific ultrasound enhanced gene transfer in vivo with novel liposomal bubbles. *J Controlled Release* **2008**, *125*, 137–144.

(8) Endo-Takahashi, Y.; Negishi, Y.; Nakamura, A.; Ukai, S.; Ooaku, K.; Oda, Y.; Sugimoto, K.; Moriyasu, F.; Takagi, N.; Suzuki, R.; Maruyama, K.; Aramaki, Y. Systemic delivery of miR-126 by miRNA-loaded Bubble liposomes for the treatment of hindlimb ischemia. *Sci. Rep.* **2014**, *4*, 1-6

(9) Jia, C.; Xu, L.; Han, T.; Cai, P.; Yu, A. C. H.; Qin, P. Generation of reactive oxygen species in heterogeneously sonoporated cells by microbubbles with single-pulse ultrasound. *Ultrasound Med Biol* **2018**, *44*, 1074–1085.

(10) Hirabayashi, F.; Iwanaga, K.; Okinaga, T.; Takahashi, O.; Ariyoshi, W.; Suzuki, R.; Sugii, M.; Maruyama, K.; Tominaga, K.; Nishihara, T.

Epidermal growth factor receptor-targeted sonoporation with microbubbles enhances therapeutic efficacy in a squamous cell carcinoma model. *PLoS One* **2017**, *12*, e0185293.

(11) Suzuki, R.; Namai, E.; Oda, Y.; Nishiie, N.; Otake, S.; Koshima, R.; Hirata, K.; Taira, Y.; Utoguchi, N.; Negishi, Y.; Nakagawa, S.; Maruyama, K. Cancer gene therapy by IL-12 gene delivery using liposomal bubbles and tumoral ultrasound exposure. *J Controlled Release* **2010**, *142*, 245–250.

(12) Yang, C.; Xiao, H.; Sun, Y.; Zhu, L.; Gao, Y.; Kwok, S.; Wang, Z.; Tang, Y. Lipid microbubbles as ultrasound-stimulated oxygen carriers for controllable oxygen release for tumor reoxygenation. *Ultrasound Med Biol* **2018**, *44*, 416–425.

(13) Krafft, M. P.; Riess, J. G. Therapeutic oxygen delivery by perfluorocarbon-based colloids. *Adv. Colloid Interface Sci.* **2021**, *294*, 102505.

(14) Gandhi, K.; Barzegar-Fallah, A.; Banstola, A.; Rizwan, S. B.; Reynolds, J. N. J. Ultrasound-Mediated Blood–Brain Barrier Disruption for Drug Delivery: A Systematic Review of Protocols, Efficacy, and Safety Outcomes from Preclinical and Clinical Studies. *Pharmaceutics* **2022**, *14*, 833.

(15) Meairs, S.; Alonso, A. Ultrasound, microbubbles and the blood-brain barrier. *Prog. Biophys. Mol. Biol.* **2007**, *93*, 354–362.

(16) McDannold, N.; Arvanitis, C. D.; Vykhodtseva, N.; Livingstone, M. S. Temporary Disruption of the Blood-Brain Barrier by Use of Ultrasound and Microbubbles: Safety and Efficacy Evaluation in Rhesus Macaques. *Cancer Res.* **2012**, *72*, 3652–3663.

(17) Choi, J. J.; Feshitan, J. A.; Baseri, B.; Wang, S.; Tung, Y. S.; Borden, M. A.; Konofagou, E. E. Microbubble-size dependence of focused ultrasound-induced blood-brain barrier opening in mice in vivo. *IEEE. Trans. Biomed. Eng.* **2010**, *57*, 145–154.

(18) Sheikov, N.; Mcdannold, N.; Sharma, S.; Hynynen, K. Effect of focused ultrasound applied with an ultrasound contrast agent on the tight junctional integrity of the brain microvascular endothelium. *Ultrasound Med Biol* **2008**, *34*, 1093–1104.

(19) Presset, A.; Bonneau, C.; Kazuyoshi, S.; Nadal-Desbarats, L.; Mitsuyoshi, T.; Bouakaz, A.; Kudo, N.; Escoffre, J. M.; Sasaki, N.

Endothelial cells, first target of drug delivery using microbubble-assisted ultrasound. *Ultrasound Med Biol* **2020,** *46*, 1565–1583.

(20) Lindner, JR.; Kaul, S. Delivery of drugs with ultrasound. *Echocardiography*. **2001**, *18*(4), 329-337.

(21) Kooiman, K.; Vos, H. J.; Versluis, M.; de Jong, N. Acoustic behavior of microbubbles and implications for drug delivery. *Adv. Drug Deliv. Rev.* **2014**, *72*, 28–48.

(22) Schutt, E. G.; Klein, D. H.; Mattrey, R. M.; Riess, J. G. Injectable microbubbles as contrast agents for diagnostic ultrasound imaging: the key role of perfluorochemicals. *Angew. Chem. Int. Ed.* **2003**, *42*, 3218–3235.

(23) Szíjjártó, C.; Rossi, S.; Waton, G.; Krafft, M. P. Effects of perfluorocarbon gases on the size and stability characteristics of phospholipid-coated microbubbles: Osmotic effect versus interfacial film stabilization. *Langmuir* **2012**, *28*, 1182–1189.

(24) Tabata, H.; Koyama, D.; Matsukawa, M.; Yoshida, K.; Krafft, M. P. Vibration characteristics and persistence of poloxamer-or phospholipid-coated single microbubbles under ultrasound irradiation. *Langmuir* **2019**, *35*, 11322-11329

(25) Epstein, P. S.; Plesset, M. S. On the Stability of Gas Bubbles in Liquid-Gas Solutions. *J. Chem. Phys.* **1950**, *18*(11), 1505-1509.

(26) Borden, M. A.; Longo, M. L. Dissolution behavior of lipid monolayer-coated, air-filled microbubbles: Effect of lipid hydrophobic chain length. **2002**, *Langmuir*, 18(24), 9225-9233.

(27) Parrales, M. A.; Fernandez, J. M.; Perez-Saborid, M.; Kopechek, J. A.; Porter, T. M. Acoustic characterization of monodisperse lipid-coated microbubbles: Relationship between size and shell viscoelastic properties. *J. Acoust. Soc. Am.* **2014**, 136, 1077-1084.

(28) van Rooij, T.; Luan, Y.; Renaud, G.; van der Steen, A. F. W.; Versluis, M.; de Jong, N.; Kooiman, K. Non-linear response and viscoelastic properties of lipid-coated microbubbles: DSPC versus DPPC. *Ultrasound Med Biol* **2015**, *41*, 1432–1445.

(29) Segers, T.; Gaud, E.; Versluis, M.; Frinking, P. High-precision acoustic measurements of the nonlinear dilatational elasticity of phospholipid coated monodisperse microbubbles. *Soft Matter* **2018**, *14*, 9550–9561.

(30) Borden, M.A.; Kruse, D. E.; Caskey, C. F.; Zhao, S.; Dayton, P. A.;

Ferrara, K. W.; Influence of lipid shell physicochemical properties on ultrasound-induced microbubble destruction. *IEEE Trans. Ultrason., Ferroelect., Freq. Contr.* **2005**, *52*(11), 1992-2002. B

(31) Raymond, J. L.; Haworth, K. J.; Bader, K. B.; Radhakrishnan, K.; Griffin, J. K.; Huang, S. L.; McPherson, D. D.; Holland, C. K. Broadband attenuation measurements of phospholipid-shelled ultrasound contrast agents. *Ultrasound Med Biol* **2014**, *40*, 410–421.

(32) Tu, J.; Guan, J.; Qiu, Y.; Matula, T. J. Estimating the shell parameters of SonoVue® microbubbles using light scattering. *J. Acoust. Soc. Am.* **2009**, *126*, 2954–2962.

(33) Faez, T.; Goertz, D.; de Jong, N. Characterization of Definity^{TM} ultrasound contrast agent at frequency range of 5-15 MHz. *Ultrasound Med Biol* **2011**, *37*, 338–342.

(34) van Rooij, T.; Luan, Y.; Renaud, G.; van der Steen, A. F. W.; de Jong, N.; Kooiman, K. Acoustical response of DSPC versus DPPC lipid-coated microbubbles. *2013 IEEE International Ultrasonics Symposium (IUS*) **2013,** 310–313.

(35) Shirazi, N. R.; Sojahrood, A. J.; Haghi, H.; de Leon, A.; Exner, A.; Kolios, M. C.; Nonlinear acoustic characterization of the shell and size engineered microbubbles and nanobubbles. *2019 IEEE International Ultrasonics Symposium (IUS)* **2019**, 1357-1360

(36) Doinikov, A. A.; Haac, J. F.; Dayton, P. A. Modeling of nonlinear viscous stress in encapsulating shells of lipid-coated contrast agent microbubbles. *Ultrasonics* **2009**, *49*, 269–275.

(37) Azami, R. H.; Aliabouzar, M.; Osborn, J.; Kumar, K. N.; Forsberg, F.; Eisenbrey, J. R.; Mallik, S.; Sarkar, K.; Material Properties, Dissolution and Time Evolution of PEGylated Lipid-Shelled Microbubbles: Effects of the Polyethylene Glycol Hydrophilic Chain Configurations. *Ultrasound Med Biol* **2022**, *48*, 1720-1732.

(38) Ando, Y.; Tabata, H.; Sanchez, M.; Cagna, A.; Koyama, D.; Krafft, M. P. Microbubbles with a self-assembled poloxamer shell and a fluorocarbon inner gas. *Langmuir* **2016**, *32*, 12461–12467.

(39) Sojahrood, A. J.; Haghi, H.; Li, Q.; Porter, T. M.; Karshafian, R.; Kolios, M. C.; Nonlinear power loss in the oscillations of coated and uncoated bubbles: Role of thermal, radiation and encapsulating shell damping at various excitation pressures, *Ultrason Sonochem* **2020**, *66.*

(40) Bali, T. G. The Generalized Extreme Value Distribution. *Econ Lett* **2003**, *79*, 423–427

(41) de Jong, N.; Hoff, L.; Skotlandt, T.; Born, N. Absorption and scatter of encapsulated gas filled microspheres: theoretical considerations and some measurements. *Ultrasonics* **1992,** *30*, 95-103

(42) Church, C. C. The effects of an elastic solid surface layer on the radial pulsations of gas bubbles. *J. Acoust. Soc. Am.* **1995**, 97, 1510-1521.

(43) Chatterjee, D.; Sarkar, K. A Newtonian rheological model for the interface of microbubble contrast agents. *Ultrasound Med Biol* **2003**, *29*, 1749–1757.

(44) Marmottant, P.; van der Meer, S.; Emmer, M.; Versluis, M.; de Jong, N.; Hilgenfeldt, S.; Lohse, D. A model for large amplitude oscillations of coated bubbles accounting for buckling and rupture. *J. Acoust. Soc. Am.* **2005**, *118*, 3499–3505.

(45) Yoshida, K.; Ebata, M.; Kaneko, C.; Zhang, Y.; Shibata, Y.; Saito, K.; Toyota, T.; Hayashi, H.; Yamaguchi, T. Fluorescence intensity changes depending on viscoelasticity of lipid shell coating microbubbles labeled with an indocyanine green derivative. *Jpn. J. Appl. Phys* **2021**, *60*, SDDE10.

(46) Eastoe, J.; Dalton, J. S. Dynamic surface tension and adsorption mechanisms of surfactants at the air-water interface. *Adv. Colloid Interface Sci.* **2000**, 85, 13-144.

(47) Svitova, T. F.; Radke, C. J. AOT and Pluronic F68 coadsorption at fluid/fluid interfaces: a continuous-flow tensiometry study. *Ind. Eng. Chem. Res.* **2005**, *44*, 1129–1138.

(48) Shekhar, H.; Smith, N. J.; Raymond, J. L.; Holland, C. K. Effect of temperature on the size distribution, shell properties, and stability of Definity®. *Ultrasound Med Biol* **2018**, *44*(2), 434-446.

(49) Xia, L.; Porter, T. M.; Sarkar, K. Interpreting attenuation at different excitation amplitudes to estimate strain-dependent interfacial rheological properties of lipid-coated monodisperse microbubbles. *J. Acoust* **2015**, *138*(6), 3994- 4003.

(50) Sojahrood, A. J.; Li, Q.; Haghi, H.; Karshafian, R.; Porter, T. M.; Kolios, M. C. Investigation of the nonlinear propagation of ultrasound through a bubbly medium including multiple scattering and bubble-bubble interaction: Theory and experiment *2017 IEEE International*

Ultrasonics Symposium (IUS), **2017**, 1-4,

(51) Sojahrood, A. J.; Earl, R.; Haghi, H.; Li, Q.; Porter, T. M.; Kolios, M. C.; Karshafian, R. Nonlinear dynamics of acoustic bubbles excited by their pressure-dependent subharmonic resonance frequency: influence of the pressure amplitude, frequency, encapsulation and multiple bubble interactions on oversaturation and enhancement of the subharmonic signal *Nonlinear Dyn,* **2021**, 103, 429-466.

(52) Sojahrood, A. J.; Li, Q.; Haghi, H.; Karshafian, R.; Porter, T. M.; Kolios, M. C. Probing the pressure dependence of sound speed and attenuation in bubbly media: Experimental observations, a theoretical model and numerical calculations. **2022**, arXiv preprint arXiv, 2211.00148

(53) Zhou, Z.; Chu, B. Light-scattering study on the association behavior of triblock polymers of ethylene oxide and propylene oxide in aqueous solution, *J. Colloid Interface Sci.* **1988**, 126(1), 171-180.

(54) Muñoz, M. G.; Monroy, F.; Ortega, F.; Rubio, R. G.; Langevin, D. Monolayers of Symmetric Triblock Copolymers at the Air−Water Interface. 1. Equilibrium Properties. *Langmuir* **1999**, 16, 1083−1093.

(55) Moghimi, S. M.; Hunter, A. C.; Dadswell, C. M.; Savay, S.; Alving, C. R.; Szebeni, J. Causative factors behind poloxamer 188 (Pluronic F68, Flocor)-induced complement activation in human sera. A protective role against poloxamer-mediated complement activation by elevated serum lipoprotein levels. *Biochim Biophys Acta.* **2004**, 1689(2), 103-13.

(56) Overvelde, M., Garbin, V., Sijl, J., Dollet, B., De Jong, N., Lohse, D. and Versluis, M. Nonlinear shell behavior of phospholipid-coated microbubbles. *Ultrasound Med Biol* **2010**, *36*(12), 2080-2092.

(57) de Jong, N.; Emmer, M.; Chin, C. T.; Bouakaz, A.; Mastik, F.; Lohse, D.; Versluis, M. “Compression-only” behavior of phospholipid-coated contrast bubbles. *Ultrasound Med Biol* **2007**, *33*, 653–656.

(58) Segers, T., De Jong, N. and Versluis, M. Uniform scattering and attenuation of acousticallysorted ultrasound contrast agents: Modeling and experiments. *J. Acoust* **2016**, *140*(4), 2506-2517

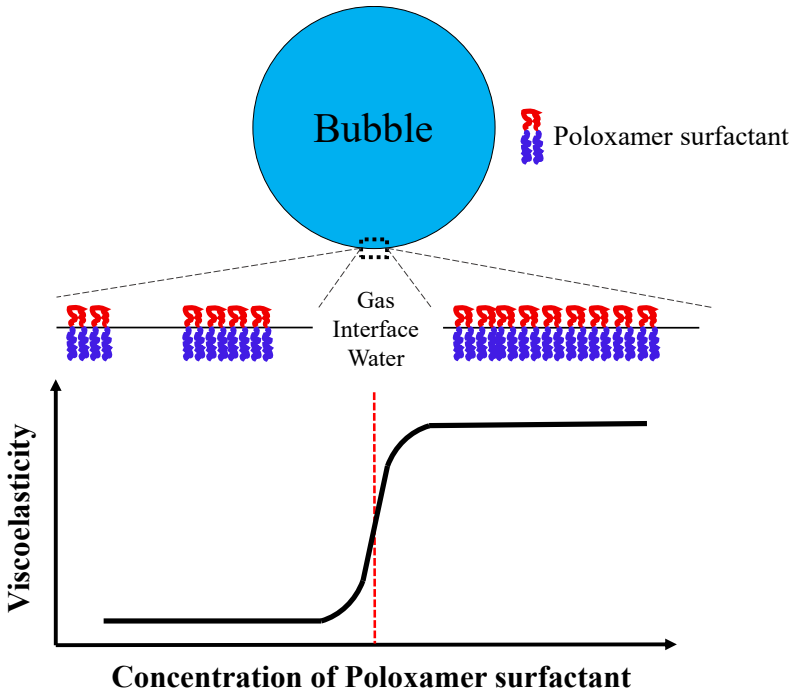

Table of graphic.